

Quantitative super-resolution imaging with qPAINT

Ralf Jungmann^{1,2,5,6}, Maier S Avendaño^{1,2,6}, Mingjie Dai^{1,3}, Johannes B Woehrstein^{1,5}, Sarit S Agasti^{1,5}, Zachary Feiger⁴, Avital Rodal⁴ & Peng Yin^{1,2}

Counting molecules in complexes is challenging, even with super-resolution microscopy. Here, we use the programmable and specific binding of dye-labeled DNA probes to count integer numbers of targets. This method, called quantitative points accumulation in nanoscale topography (qPAINT), works independently of dye photophysics for robust counting with high precision and accuracy over a wide dynamic range. qPAINT was benchmarked on DNA nanostructures and demonstrated for cellular applications by quantifying proteins *in situ* and the number of single-molecule FISH probes bound to an mRNA target.

Optical super-resolution microscopy is revolutionizing the way we study biology. It allows researchers to achieve a spatial resolution below the diffraction limit of light¹, providing insights that were previously impossible². Super-resolution studies often focus on the visualization of synthetic or cellular structures with sub-diffraction spatial resolution. However, data sets obtained by stochastic switching and readout methods^{3–5} contain a wealth of information that can be explored for quantitative studies^{6–13} beyond ‘just’ binning molecule localizations for spatial visualization. These counting techniques typically rely on complex modeling of blinking properties for target-bound fluorescent dyes. However, with current methods it is difficult to accurately and precisely quantify the number of target-bound fluorophores, especially for a large number of fluorescent proteins or dyes in dense clusters. First, the dyes typically have complex, environmentally sensitive photophysics that are difficult to model. Different switching properties for dissimilar dyes further complicate multiplexed quantitative imaging¹⁴. Furthermore, irregular sample illumination or varying excitation and activation intensities can lead to variation in switching kinetics and thus inaccurate quantification¹³. Additionally, target-bound dyes can be bleached prematurely, before sufficient localizations are collected to allow for accurate and precise quantification.

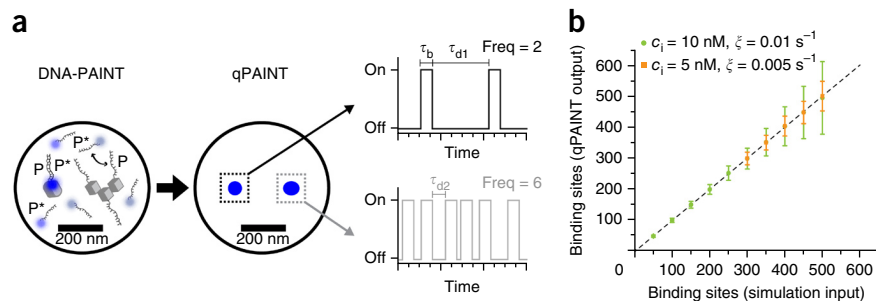
We introduce a simple and robust quantitative super-resolution method called quantitative PAINT (or qPAINT) based on DNA-PAINT^{15–19}. Instead of relying on stochastic switching of target-bound dyes^{3,4}, DNA-PAINT achieves apparent blinking of targets via transient binding of free-floating dye-labeled ‘imager’ strands to complementary target-bound ‘docking’ strands. By analyzing the predictable binding kinetics between the imager and docking strands, qPAINT counts the number of targets without spatially resolving them. As compared to existing quantification methods, qPAINT has two unique features: it explicitly decouples blinking from dye photophysics and it is immune to photobleaching (as dye-labeled imager strands are continuously replenished from the solution).

Thanks to these features, qPAINT represents a conceptual framework that can simultaneously achieve high accuracy, precision, a wide dynamic range, robustness, and multiplexing capability for quantifying the number of labeled targets. More specifically, by explicitly avoiding analyzing the hard-to-predict and illumination-dependent photophysical kinetics of dyes, qPAINT achieves high quantification accuracy. Immunity to photobleaching permits arbitrarily long imaging time and the collection of a large number of blinking events, leading to high counting precision. The easily adjustable influx rate of the imager strands makes such high accuracy and precision achievable over a wide dynamic range. Consistent, predictable, and easily calibratable (when required) binding kinetics allows qPAINT to work robustly under diverse conditions and with different dyes. Finally, because it decouples the apparent blinking from the photophysical properties of dyes, qPAINT is easily multiplexable (spectrally and sequentially¹⁷).

Figure 1 illustrates the principle of qPAINT with the example of protein quantification in resolution-limited spots in a fixed cell. The region in **Figure 1a** consists of one protein spaced about 200 nm away from a small cluster formed by three proteins (which are spaced ~5 nm apart). Current super-resolution techniques fall short of resolving individual proteins in the small cluster. Thus, simple spatial counting would underestimate the total number of proteins. However, by analyzing the predictable and programmable binding kinetics of imager strands in DNA-PAINT rather than spatially resolving individual targets, it is possible to quantify integer numbers of molecules in these resolution-limited areas. Single-molecule DNA hybridization and dissociation can be described using a simple kinetic model with a second-order association rate k_{on} and a first-order dissociation rate k_{off} . These kinetic constants determine the fluorescence on- and off-times (τ_{b} for bright-time and τ_{d} for dark-time, respectively). τ_{b} is linked to k_{off} via $\tau_{\text{b}} = k_{\text{off}}^{-1}$ and τ_{d} is linked to the influx rate of imager strands $\xi = k_{\text{on}} \times c_{\text{i}}$ by $\tau_{\text{d}} = (k_{\text{on}} \times c_{\text{i}})^{-1} = \xi^{-1}$, where

¹Wyss Institute for Biologically Inspired Engineering, Harvard University, Boston, Massachusetts, USA. ²Department of Systems Biology, Harvard Medical School, Boston, Massachusetts, USA. ³Harvard Program in Biophysics, Harvard University, Boston, Massachusetts, USA. ⁴Rosenstiel Basic Medical Sciences Research Center, Department of Biology, Brandeis University, Waltham, Massachusetts, USA. ⁵Present addresses: Max Planck Institute of Biochemistry and Ludwig Maximilian University of Munich, Munich, Germany (R.J. and J.B.W.); Jawaharlal Nehru Centre for Advanced Scientific Research (JNCASR), Jakkur, Bangalore, India (S.S.A.). ⁶These authors contributed equally to this work. Correspondence should be addressed to P.Y. (py@hms.harvard.edu).

Figure 1 | qPAINT principle. (a) In DNA-PAINT, fluorescently labeled ‘imager’ strands (P^*) transiently bind from solution to complementary ‘docking’ strands (P) attached to a target. Intensity vs. time traces show characteristic fluorescence on- and off-times (τ_b and τ_d , respectively). qPAINT uses the predictable blinking kinetics to deduct molecule numbers. (b) The number of binding sites can be calculated given a known probe influx rate $\xi = k_{on} \times c_i$. Stochastic simulations of DNA-PAINT binding events show a linear relationship between simulated and ‘measured’ numbers of binding sites (mean \pm s.d.). The counting precision for a given number of sites is dependent on the probe influx rate ξ (green, 0.01 s^{-1} ; orange, 0.005 s^{-1}).



c_i is the imager strand concentration. If a single protein molecule labeled with a single docking strand ‘blinks’ with a frequency of 2 in a certain time interval, then three molecules (containing three docking sites) will blink with three times the frequency, given a constant influx rate ξ (Fig. 1a). To practically quantify the number of binding sites from the intensity versus time traces, we first determine the mean dark-time τ_{d^*} from the cumulative distribution function (Supplementary Fig. 1) in an area of interest, and then calculate the number of binding sites as $(k_{on} \times c_i \times \tau_{d^*})^{-1} = (\xi \times \tau_{d^*})^{-1}$.

We first performed qPAINT *in silico* by stochastically simulating DNA-PAINT data and plotting the results obtained by qPAINT versus the ‘true’ molecule number used as input (Fig. 1b). The linear relationship between the results and the true molecule number over a wide range of binding sites shows that counting with qPAINT is feasible (see Supplementary Fig. 2 for discussion regarding binding frequency readout). qPAINT’s counting precision ($1 - c_v$ with $c_v = \sigma/\mu$: coefficient of variation with σ/μ s.d. and mean, respectively) can be increased by optimizing the probe influx rate ξ or extending image acquisition (Supplementary Fig. 3).

Next, we experimentally benchmarked qPAINT *in vitro* and compared it to our *in silico* results. We adopted a DNA origami²⁰-based imaging quality benchmark platform and an accompanying drift correction and high-resolution image analysis

method²¹. The origami was designed to display 12 binding sites that can be visually separated using an advanced image analysis method that can achieve ultra-high-resolution imaging to discretely visualize each target in a densely packed cluster²¹ (Fig. 2a, design details in Supplementary Fig. 4). The visually counted (‘ground truth’) number of sites can be compared to the qPAINT analysis for the same structure, omitting any a priori spatial information (Fig. 2b). High-resolution DNA-PAINT imaging revealed that not all origami showed 12 binding sites (Fig. 2b; see also Supplementary Fig. 5), likely resulting from missing docking strands¹⁵ (see Supplementary Fig. 6 for incorporation efficiency measurement). Comparing qPAINT *in vitro* and *in silico* (Fig. 2c) versus the ground truth showed good agreement (90% precision, 97% accuracy). Adjusting the imager influx rate to $\xi = 0.03 \text{ s}^{-1}$ and extending image acquisition time further increased the precision and accuracy to 95.4% and 99.6%, respectively (Fig. 2c and Supplementary Fig. 7). This then allowed us to distinguish between integer numbers of sites (i.e. between 9, 10, 11, and 12, Fig. 2d).

While counting a few molecules is possible using stepwise photobleaching approaches²² or photon statistics²³, these approaches are less effective for counting higher fluorophore densities²⁴. For this reason, we sought to demonstrate similar qPAINT performance for a higher target density. Grouping four DNA

Figure 2 | qPAINT *in vitro* benchmarking.

(a) DNA origami structure with 12 designed docking sites. (b) DNA-PAINT image of the structures. (c) Visual counting (x-axis), *in silico* simulation (gray), and *in vitro* experimental qPAINT data (orange and green) are in good agreement (97% accuracy and 90% precision for $\xi = 0.02 \text{ s}^{-1}$ and 25 min imaging time; 99.6% accuracy and 95.4% precision for $\xi = 0.03 \text{ s}^{-1}$ and 166 min imaging time; error bars, 1 s.d.). (d) Distributions plotted from data in c (green data points) demonstrate qPAINT’s ability to distinguish between integer numbers of binding sites (i.e., 9 vs. 10 vs. 11 vs. 12; Tukey *post hoc* test: $F_{3,605} = 1,032.52$, $*P < 0.01$, Supplementary Fig. 7). (e) Dynamic range. Same DNA-PAINT data set as in c (orange data points) reanalyzed by grouping four DNA origami structures together. (f) Comparison between visual counting (x-axis) and *in vitro* (orange) qPAINT analysis; error bars, 1 s.d. (g) *In silico* analysis of the counting error (coefficient of variation, c_v) dependency on the number of binding sites and imager strand influx rate. Tuning ξ (experimentally adjustable over a wide range) can reach optimal conditions with low counting errors (<10%) for virtually any number of bindings sites. (h) Multiplexed qPAINT. Three distinct DNA origami structures (similar to those in c) with orthogonal docking strand sequences (red P1, green P3 and blue P5; error bars, 1 s.d.) were imaged sequentially using Exchange-PAINT. Inset shows qPAINT analysis on 11 binding sites structures. Scale bars: 100 nm (b,h), 500 nm (e).

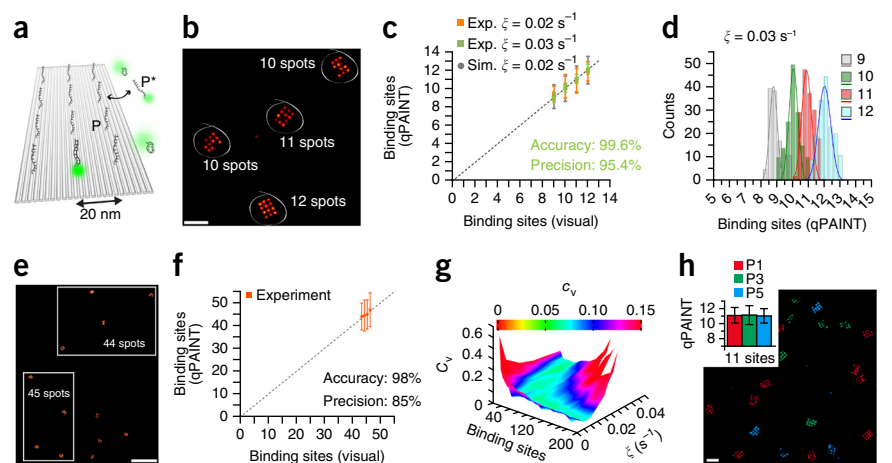
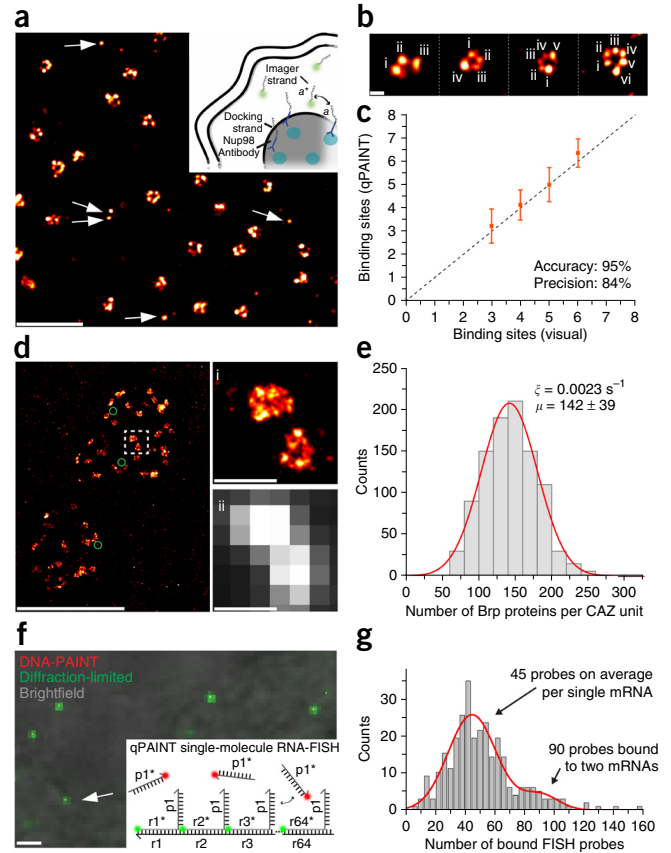


Figure 3 | qPAINT *in situ*. (a–c) qPAINT *in situ* benchmarking with Nup98. (a) DNA-PAINT image of Nup98 proteins in NPCs. Inset: labeling and imaging schematic for NPC proteins. Single targets (marked with arrows) are used for influx rate calibration. (b) NPC structures displaying three, four, five, and six distinct Nup98 protein clusters were respectively grouped for qPAINT analysis. (c) Comparison between visual counting (*x*-axis) and qPAINT data (orange); error bars, 1 s.d. (d,e) Brp qPAINT experiments. (d) DNA-PAINT image of *Drosophila* NMJs obtained by using secondary DNA-antibody conjugates and primary monoclonal antibodies against Brp^{Nc82}. Zoomed-in view (i, DNA-PAINT; ii, diffraction limited) of the highlighted area in d showing two separate CAZ units (assemblies of Brp proteins into multiprotein clusters¹²). Green circles indicate single targets. (e) qPAINT quantification (*n* = 981) indicating that the average number of Brp molecules per CAZ unit is 142 ± 39 (mean \pm s.d.). (f,g) smFISH qPAINT experiments. (f) SUZ12 mRNAs molecules are tagged using single-stranded oligonucleotides with binding sequences unique to a part of the target mRNA (r1*–r64*), a fixed Cy3B label, and a single-stranded DNA-PAINT docking strand (p1). (g) qPAINT quantification (*n* = 301) yields ~45 probes bound to a single mRNA molecule (~90 probes for two mRNAs), revealing ~70% hybridization efficiency of the FISH probes to the mRNA target. Scale bars: 500 nm (a, insets i and ii in d), 50 nm (b), 1 μ m (d,f).



origami from the previous data set into one region of interest for qPAINT analysis allowed us to assay qPAINT's performance for counting 48 sites (Fig. 2e; note that spatial information was still disregarded). Again, qPAINT versus ground truth analysis showed good agreement (Fig. 2f; 98% accuracy, 85% precision). Additionally, we performed qPAINT on DNA origami with 12, 48, and 150 binding sites, respectively, yielding similar performance (see Supplementary Figs. 4 and 8 for design and results).

Next, we performed an *in silico* study to determine the counting error for a given set of binding sites and imager strand influx rate ξ (Fig. 2g). The results show that ξ can be tuned to select an optimal 'working' point depending on the expected number of binding sites, thus achieving high counting precision over a wide dynamic range. Specifically, one should be able to obtain counting errors below 10% independent of the number of binding sites. Finally, we demonstrated the ability of qPAINT to count multiple target species in the same sample with similar performance by performing Exchange-PAINT¹⁷ on three distinct DNA origami structures in the same sample (Fig. 2h) using orthogonal imager strand sequences.

Moving from a clean *in vitro* to a more complex *in situ* environment, we next evaluated qPAINT on DNA origami structures bound to cell surface proteins or microinjected in the nuclear and cytoplasmic regions of fixed cells (Supplementary Fig. 9). In both cases, qPAINT performed favorably, achieving accuracy and precision similar to those for the *in vitro* DNA origami results. Comparing nuclear and cytoplasmic counting results yielded similar numbers, demonstrating the consistent binding kinetics of qPAINT in different locations in fixed cells and suggesting its applicability, for example, for counting proteins or DNA or RNA molecules *in situ*.

We next benchmarked qPAINT's performance *in situ* by quantifying the number of individual units that form the symmetrical ring structure of the nuclear pore complexes (NPCs) by targeting the nucleoporin Nup98 (anchored mainly to the inner ring of the NPC^{25,26}) in U2OS cells using monoclonal primary antibodies directly conjugated to docking strands (Fig. 3a). Due to variation of Nup98 protein units present in each NPC and potentially imperfect antibody labeling (Fig. 3a), not all complexes show the same number of individual proteins units (Fig. 3b and Supplementary Fig. 10). We first used single isolated Nup98 protein clusters as

calibration for the probe influx rate. The association rate was determined by using the mean value from the Gaussian fitting of the dark-time distribution from the individual protein localizations (Fig. 3a). We subsequently grouped NPC structures according to their number of visible Nup98 protein units. We then plotted for each group the distribution obtained by qPAINT versus the visually determined ground truth and we obtained 95% accuracy and 84% precision (Fig. 3c).

We then applied qPAINT to quantify the number of single Bruchpilot proteins (Brp), which are structural and functional components of the cytomatrix at the synaptic active zone (CAZ) in the *Drosophila* neuromuscular junction (NMJ)²⁷. Here, we used monoclonal primary antibodies (Brp^{Nc82})^{12,27} and DNA-conjugated secondary antibodies for labeling. Similarly to what was done in a previous study¹², we defined a CAZ unit as an interconnected region of Brp molecules with an elliptical shape (Fig. 3d, i, and Supplementary Fig. 11). Subsequent qPAINT yielded 142 ± 39 (mean \pm s.d.) Brp molecules per CAZ, consistent with previously reported numbers using quantitative dSTORM¹² (Fig. 3e). Note that more than one secondary antibody can be bound per primary antibody. This, together with the variability of antibodies bound per subunit, will lead to a larger 'labeling' variability. However, unlike previous work involving elaborate calibration using antibody titration¹², qPAINT simply uses single isolated targets to calibrate the influx rate as described above.

Finally, we applied qPAINT to quantify the number of probes bound to an mRNA target (SUZ12) in single-molecule fluorescence *in situ* hybridization (smFISH) experiments (Fig. 3f; see Supplementary Fig. 12 for a larger view). We used a probe set of 64 smFISH probes²⁸ consisting of a 5'-Cy3B label and a docking

strand on the 3' end (inset Fig. 3f). After cell fixation, labeling²⁹ (see Online Methods for details), and imaging, colocalization between Cy3B and DNA-PAINT was observed (Fig. 3f). Subsequent qPAINT analysis yielded—for the first time, to our knowledge—the number of *in situ*-bound smFISH probes per mRNA molecule. The bimodal distribution showed a first peak at ~45 and a second peak at ~90, consistent with one and two mRNA molecules in a resolution-limited area, respectively (Fig. 3g). Note that counting less than the designed 64 smFISH strands is expected, as it is likely that not all FISH probes were bound at each mRNA molecule. This experiment thus indicates that ~70% of all designed smFISH probes were bound to their targets, with a variance of ~36%.

As qPAINT decouples blinking kinetics from dye photophysics and is immune to photobleaching (see Supplementary Fig. 13), it avoids typical 'undercounting' errors due to already photobleached or 'inactive' dye labels, as well as 'overcounting' errors due to blinking artifacts that are unaccounted for^{10,30}. qPAINT works robustly under diverse experimental conditions with consistent high accuracy and precision (see Supplementary Fig. 14 for day-to-day reproducibility). Although qPAINT performs robustly, it is still reliant on stoichiometric labeling of protein targets. Imperfect labeling could potentially lead to undercounting. Similarly to the approach taken with the previous quantitative approach, dSTORM¹², we opted to use standard immunostaining to label endogenous protein targets with antibodies and we obtained comparable quantification results, but with a simpler *in situ* calibration using isolated single targets. For future quantification of proteins in compact clusters, alternative labeling techniques (for example, nanobodies³¹, aptamers³², modified amino acids³³, or small-molecule binders) need to be developed. In our present work, we demonstrated qPAINT using DNA-PAINT, but the general concept may be generalized to other PAINT methods (for example, recently developed IRIS probes³⁴).

METHODS

Methods and any associated references are available in the [online version of the paper](#).

Note: Any Supplementary Information and Source Data files are available in the [online version of the paper](#).

ACKNOWLEDGMENTS

We thank M.T. Strauss and J. Lara for help with DNA origami design and J. Werbin (Department of Systems Biology, Harvard Medical School) for the donation of CHO cells and fruitful discussions. We also thank A. Raj for providing the smFISH sequences, F. Schueder for initial Brp imaging experiments, and H. Soundararajan and J. Paulson for fruitful discussions. This work is supported by a National Institutes of Health (NIH) Director's New Innovator Award (1DP20D007292), an NIH Transformative Research Award (1R01EB018659), an NIH grant (5R21HD072481), an Office of Naval Research (ONR) Young Investigator Program Award (N000141110914), ONR grants (N000141010827 and N000141310593), a National Science Foundation (NSF) Faculty Early Career Development Award (CCF1054898), an NSF grant (CCF1162459) and a Wyss Institute for Biologically Engineering Faculty Startup Fund to P.Y., and a Pew Scholar Award to A.R. The BRP antibodies were obtained from the Developmental Studies Hybridoma Bank, created by the NICHD of the NIH. R.J. acknowledges support from the Alexander von Humboldt Foundation through a Feodor-Lynen Fellowship. M.S.A. and M.D. acknowledge support from HHMI International Student Research Fellowships.

AUTHOR CONTRIBUTIONS

R.J. and M.S.A. conceived of the study, designed and performed the experiments, analyzed the data, developed software, and wrote the manuscript. M.D. developed software and wrote the manuscript. J.B.W. helped with *in vitro* experimental design and wrote the manuscript. S.S.A. helped with DNA-dye conjugation and developed the antibody labeling protocol. Z.F. and A.R. helped with Brp experiments. P.Y. conceived of and supervised the study, interpreted the data and wrote the manuscript. All authors reviewed and approved the manuscript.

COMPETING FINANCIAL INTERESTS

The authors declare competing financial interests: details are available in the [online version of the paper](#).

Reprints and permissions information is available online at <http://www.nature.com/reprints/index.html>.

- Hell, S.W. *Nat. Methods* **6**, 24–32 (2009).
- Xu, K., Zhong, G. & Zhuang, X. *Science* **339**, 452–456 (2013).
- Betzig, E. *et al. Science* **313**, 1642–1645 (2006).
- Rust, M.J., Bates, M. & Zhuang, X. *Nat. Methods* **3**, 793–795 (2006).
- Sharonov, A. & Hochstrasser, R.M. *Proc. Natl. Acad. Sci. USA* **103**, 18911–18916 (2006).
- Lee, S.H., Shin, J.Y., Lee, A. & Bustamante, C. *Proc. Natl. Acad. Sci. USA* **109**, 17436–17441 (2012).
- Renz, M., Daniels, B.R., Vamosi, G., Arias, I.M. & Lippincott-Schwartz, J. *Proc. Natl. Acad. Sci. USA* **109**, E2989–E2997 (2012).
- Endesfelder, U. *et al. Biophys. J.* **105**, 172–181 (2013).
- Puchner, E.M., Walter, J.M., Kasper, R., Huang, B. & Lim, W.A. *Proc. Natl. Acad. Sci. USA* **110**, 16015–16020 (2013).
- Duricic, N., Laparra-Cuervo, L., Sandoval-Alvarez, A., Borbely, J.S. & Lakadamyali, M. *Nat. Methods* **11**, 156–162 (2014).
- Zhao, Z.W. *et al. Proc. Natl. Acad. Sci. USA* **111**, 681–686 (2014).
- Ehmann, N. *et al. Nat. Comm.* **5**, 4650 (2014).
- Nieuwenhuizen, R.P. *et al. PLoS ONE* **10**, e0127989 (2015).
- Dempsey, G.T., Vaughan, J.C., Chen, K.H., Bates, M. & Zhuang, X. *Nat. Methods* **8**, 1027–1036 (2011).
- Jungmann, R. *et al. Nano Lett.* **10**, 4756–4761 (2010).
- Lin, C. *et al. Nat. Chem.* **4**, 832–839 (2012).
- Jungmann, R. *et al. Nat. Methods* **11**, 313–318 (2014).
- Iinuma, R. *et al. Science* **344**, 65–69 (2014).
- Schlichthaerle, T., Strauss, M.T., Schueder, F., Woehrstein, J.B. & Jungmann, R. *Curr. Opin. Biotechnol.* **39**, 41–47 (2016).
- Rothmund, P.W. *Nature* **440**, 297–302 (2006).
- Dai, M., Jungmann, R. & Yin, P. *Nat. Nanotechnol.* (in the press).
- Ulbrich, M.H. & Isacoff, E.Y. *Nat. Methods* **4**, 319–321 (2007).
- Ta, H., Kiel, A., Wahl, M. & Herten, D.P. *Phys. Chem. Chem. Phys.* **12**, 10295–10300 (2010).
- Coffman, V.C. & Wu, J.Q. *Trends Biochem. Sci.* **37**, 499–506 (2012).
- Hoelz, A., Debler, E.W. & Blobel, G. *Annu. Rev. Biochem.* **80**, 613–643 (2011).
- Strambio-De-Castillia, C., Niepel, M. & Rout, M.P. *Nat. Rev. Mol. Cell Biol.* **11**, 490–501 (2010).
- Fouquet, W. *et al. J. Cell Biol.* **186**, 129–145 (2009).
- Raj, A., van den Bogaard, P., Rifkin, S.A., van Oudenaarden, A. & Tyagi, S. *Nat. Methods* **5**, 877–879 (2008).
- Shaffer, S.M., Wu, M.T., Levesque, M.J. & Raj, A. *PLoS ONE* **8**, e75120 (2013).
- Endesfelder, U. *et al. Molecules* **16**, 3106–3118 (2011).
- Ries, J., Kaplan, C., Platonova, E., Eghlidi, H. & Ewers, H. *Nat. Methods* **9**, 582–584 (2012).
- Opazo, F. *et al. Nat. Methods* **9**, 938–939 (2012).
- Milles, S. *et al. J. Am. Chem. Soc.* **134**, 5187–5195 (2012).
- Kiuchi, T., Higuchi, M., Takamura, A., Maruoka, M. & Watanabe, N. *Nat. Methods* **12**, 743–746 (2015).

ONLINE METHODS

Materials. Non-modified and amino-modified DNA oligonucleotides were purchased from Integrated DNA Technologies (Coralville, IA). Fluorescently-labeled DNA oligonucleotides were purchased from Biosynthesis (Lewisville, TX). Biotinylated monoclonal antibody against EGF receptor was purchased from Cell Signaling (Cat. No. 6627, Danvers, MA). Streptavidin was purchased from Invitrogen (S-888, Carlsbad, CA). Bovine serum albumin (BSA), BSA-Biotin and Triton X-100 was obtained from Sigma Aldrich (A8549, St. Louis, MO). Whole cell blue stain was obtained from Thermo Scientific (8403501, Rockford, IL). Glass slides and coverslips were purchased from VWR (Radnor, PA). Lab-Tek II chambered coverglass was purchased from Thermo Fisher Scientific (Billerica, MA). M13mp18 scaffold was obtained from New England BioLabs (Ipswich, MA). Freeze 'N Squeeze columns were ordered from Bio-Rad (Hercules, CA). Paraformaldehyde and glutaraldehyde were obtained from Electron Microscopy Sciences (Hatfield, PA). Protocatechuic acid (PCA), Protocatechuate-3,4-dioxygenase (PCD), and Trolox (TX) were purchased from Sigma-Aldrich (37580-25G-F (PCA), P8279-25UN (PCD), 238813-5G (TX)) (St. Louis, MO).

Four buffers were used for sample preparation and imaging: buffer A (10 mM Tris-HCl, 100 mM NaCl, 0.05% Tween-20, pH 7.5), buffer B (5 mM Tris-HCl, 10 mM MgCl₂, 1 mM EDTA, 0.05% Tween-20, pH 8), buffer B⁺ (5 mM Tris-HCl, 10 mM MgCl₂, 1 mM EDTA, 0.05% Tween-20, pH 8, supplemented with 1 mM PCA, 1 mM PCD, and 1 mM TX), and buffer C (1× PBS, 500 mM NaCl, pH 8).

Super-resolution optical setup. Fluorescence imaging was carried out on an inverted Nikon Eclipse Ti microscope (Nikon Instruments, Melville, NY) with the Perfect Focus System, applying an objective-type TIRF configuration using a Nikon TIRF illuminator with an oil-immersion objective (CFI Apo TIRF 100×, NA 1.49, Oil), corresponding to a final pixel size of 160 nm. Three lasers were used for excitation: 488 nm (200 mW nominal, Coherent Sapphire, Santa Clara, CA), 561 nm (200 mW nominal, Coherent Sapphire) and 647 nm (300 mW nominal, MBP Communications, Canada). The laser beam was passed through cleanup filters (ZT488/10, ZET561/10, and ZET640/20, Chroma Technology, Bellows Falls, VT) and coupled into the microscope objective using a multi-band beam splitter (ZT488rdc/ZT561rdc/ZT640rdc, Chroma Technology). Fluorescence light was spectrally filtered with emission filters (ET525/50m, ET600/50m, and ET700/75m, Chroma Technology) and imaged on an EMCCD camera (iXon X3 DU-897, Andor Technologies, North Ireland).

Confocal setup. Confocal imaging was carried out on a Zeiss Axio Observer with LSM 710 scanning laser confocal system (Zeiss, Thornwood, NY) using the following excitation and emission lines: Whole cell blue stain: 25 mW Argon laser (458/488/514 nm) and 490–560 nm emission filter. Cy3: 20 mW DPSS laser (561 nm) and 563–593 nm emission filter.

Data analysis. Super-resolution DNA-PAINT images were reconstructed using custom-programmed software written in either LabVIEW^{15,17} or MATLAB²¹ for spot-finding and 2D-Gaussian fitting¹⁷. Drift correction and super-resolution imaging analysis for the 20 nm grid origami sample was performed using custom

MATLAB software to visually separate the binding sites²¹. Subsequent qPAINT analysis was performed using a custom-written software implemented in LabVIEW. Both reconstruction and analysis programs are available upon request. After single-molecule reconstruction, the qPAINT analysis software uses a region of interest as input (either automatically or interactively selected) for the binding kinetics analysis. The software determines the mean dark time τ_{d^*} by first creating a cumulative distribution function (cdf) from all dark times t and subsequently fitting this distribution to a single exponential function¹⁵:

$$P(t) = 1 - \exp(-t/\tau_{d^*}),$$

with P representing the binding probability for a DNA-PAINT imaging probe at time t after a previous unbinding event. Finally—after calibrating the imager probe influx rate $\xi = k_{\text{on}} \times c_i$ from a known calibration sample (i.e. previously established from experiments under similar conditions or *in situ* DNA origami calibration standards)—the number of binding sites in the selected region of interest is obtained by

$$\text{binding sites} = \frac{1}{\tau_{d^*} \cdot \xi}$$

qPAINT data simulation. *In silico* qPAINT experiments were performed using COPASI³⁵. In brief, a bimolecular chemical reaction model—modeling DNA hybridization and dissociation reactions—with two species (docking and imager strands) and two rate constants (association rate k_{on} and dissociation rate k_{off}) was used. Using a direct stochastic solver, we performed time-lapsed simulations that yielded binarized single-molecule intensity versus time traces. These traces were then subjected to the same qPAINT analysis software that was used to analyze the experimental data (see above). Simulation parameters were selected in accordance to the respective experimental conditions.

Simulation conditions: for the simulation in **Figure 1b**, two probe influx rates (0.005 s⁻¹ and 0.01 s⁻¹) were used, corresponding to 5 nM and 10 nM imager strand concentration at a constant association rate k_{on} of 10⁶ M⁻¹s⁻¹. Simulations were run for 15,000 “frames” at a sampling interval (or “integration” time) of 0.1 s. 200 simulations per data point were performed (mean and s.d. are plotted in **Fig. 1b**). More detailed simulation conditions for simulations accompanying experimental data are given in the following paragraphs.

DNA origami self-assembly. DNA origami structures displaying 12, 44, 48 and 150 DNA-PAINT docking sites were self-assembled in a one-pot reaction with 50 μ l total volume containing 10 nM scaffold strand M13mp18, 100 nM folding staples, 100 nM biotinylated staples, and 1 μ M DNA-PAINT docking staple strands in folding buffer (1× TE Buffer with 12.5 mM MgCl₂). The solution was annealed using a thermal ramp cooling from 90 °C to 20 °C over the course of 1.5 h. After self-assembly, structures were purified by agarose gel electrophoresis (2% agarose, 0.5× TBE, 10 mM MgCl₂, 0.5× SybrSafe) at 4.5 V/cm for 1.5 h. Gel bands were cut, crushed and filled into a Freeze 'N Squeeze column and spun for 5 min at 800 × g at 4 °C. After this, structures were ready for microscopy sample preparation and image acquisition.

DNA sequences. 20 nm grid structures can be found in **Supplementary Table 1**. Staple sequences for 12 docking sites origami can be found in **Supplementary Table 2**. Staple sequences for 48 docking sites origami can be found in **Supplementary Table 3**. Staple sequences for 150 docking sites origami can be found in **Supplementary Table 4**. Staple sequences for 20 nm grid structures with fixed Cy3 dyes can be found in **Supplementary Table 5**. Staple sequences for 44 docking sites origami with fixed Cy3 dyes can be found in **Supplementary Table 6**. M13mp18 scaffold sequence for DNA origami structures can be found in **Supplementary Table 7**. Sequences for FISH-PAINT probes can be found in **Supplementary Table 8**. DNA-PAINT docking and imager sequences and biotin docking sequence can be found in **Supplementary Table 9**.

Sample preparation, imaging, and analysis of DNA origami structures. *Sample preparation.* For sample preparation, a piece of coverslip (No. 1.5, 18 × 18 mm², ~0.17 mm thick) and a glass slide (3 × 1 inch², 1 mm thick) were sandwiched together by two strips of double-sided tape to form a flow chamber with inner volume of ~20 μl. First, 20 μl of biotin-labeled bovine albumin (1 mg/ml, dissolved in buffer A) was flown into the chamber and incubated for 2 min. The chamber was then washed using 40 μl of buffer A. 20 μl of streptavidin (0.5 mg/ml, dissolved in buffer A) was then flown through the chamber and allowed to bind for 2 min. After washing with 40 μl of buffer A and subsequently with 40 μl of buffer B, 20 μl of biotin labeled DNA structures (~300 pM concentration) in buffer B were finally flown into the chamber and incubated for 5 min. The chamber was washed using 40 μl of buffer B⁺ for *in vitro* imaging of 20 nm grid structures and buffer B for all other *in vitro* DNA origami experiments.

Imaging conditions. The imaging buffer contained 10 nM (Fig. 2b,e) or 15 nM (Fig. 2c,d) Cy3B-labeled imager strands in buffer B⁺, or 20 nM Atto 655-labeled imager strands in buffer B (Supplementary Fig. 8). Imaging chambers were sealed with epoxy before imaging. Image acquisition was carried out with a CCD readout bandwidth of 3 MHz at 14 bit and 5.1 pre-amp gain. No EM gain was used. Imaging was performed using TIR illumination with an excitation intensity of ~5 mW using the 561 nm laser line (Fig. 2b–e) or ~40 mW using the 647 nm laser line (Supplementary Fig. 8). 15,000 frames at 10 Hz frame rate were acquired (Fig. 2b,e,h and Supplementary Fig. 8). 50,000 frames at 5 Hz frame rate were acquired (Fig. 2c green data points).

Data analysis. Super-resolution images were reconstructed in either custom LabVIEW or MATLAB software as described above. qPAINT analysis on DNA origami structures was performed interactively by selecting a region of interest that was large enough to fully comprise a single DNA origami (compare gray “ROIs” (regions of interest) in Fig. 2b). First, 100 random DNA origami structures displaying the same number of binding sites (i.e. 10 spots) were used to calibrate the probe influx rate ξ . For the imaging conditions used, a probe influx rate of 0.02 s⁻¹ was determined (Fig. 2c,f, orange data points, and Fig. 2h) and 0.03 s⁻¹ (Fig. 2c, green data points). These influx rates were then used to perform qPAINT analysis on all DNA origami structures in the sample. qPAINT analysis for the sample in **Supplementary Figure 8** was performed similarly. Here, the probe influx rate was determined by assuming that the 12 binding site origami structures carry on average 10.5 binding sites (determined by visual

counting of similar structures in Fig. 2b). Here, a probe influx rate of 0.0201 s⁻¹ was determined for the imaging conditions used in this experiment.

Simulation conditions. qPAINT simulations for **Figure 2c** were performed using 9, 10, 11, or 12 binding sites as model input in combination with association and dissociation rates obtained from the experimental data. qPAINT simulations used in **Supplementary Figure 8** were performed in a similar fashion, here, however, using a normal distribution of binding sites with means determined from the experimental data. s.d. of the normal distribution were scaled based on the simulated mean value taking the 12 binding site data from **Figure 2b** as input. qPAINT simulations for **Figure 2g** were performed similarly to simulations in **Figure 1b**. Here, binding sites ranging from 2 to 200 binding sites and probe influx rates ranging from 0.001 s⁻¹ to 0.05 s⁻¹ were used to perform 200 stochastic simulations per value pair. After analysis, the coefficient of variation ($c_v = \sigma/\mu$), reflecting the counting error, is plotted against the number of binding sites and probe influx rate. As before, 15,000 frames at an “integration time” of 0.1 s are simulated.

Sample preparation, acquisition, and analysis of artificial receptor clusters on cell surfaces. *Sample preparation.* CHO cells were transiently transfected with the construct encoding a human wild-type EGFR fused with the fluorescent protein mEos (pQCEGFRmEoS; a kind gift from Jeff Werbin, Harvard Medical School) using Lipofectamine (Invitrogen) according to the manufacturer’s instructions. Briefly, for each transfection reaction, 10 μL Lipofectamine was incubated with 250 μL Opti-MEM for 10 min. Next, 4 μg of EGFR-mEos vector plasmid was added and incubated for 30 min. This mixture was added to cells and incubated overnight. Transfections were carried out when CHO cells were at 90% confluence. After 24 h, approximately 30% confluence cells per well were seeded into Lab-Tek II chambers for 24 h before fixation. EGF receptors were immunostained using the following procedure: washing in PBS; fixation in a mixture of 3% paraformaldehyde and 0.1% glutaraldehyde in PBS for 10 min; three washes with PBS; reduction with ~1 mg/ml NaBH₄ for 7 min; three washes with PBS; permeabilization with 0.25% (v/v) Triton X-100 in PBS for 10 min; three washes with PBS; blocking with 3% (w/v) bovine serum albumin for 30 min and staining overnight with the biotinylated EGFR monoclonal antibody (diluted to 10 μg/ml in 5% BSA); three washes with PBS; incubation with 20 μg/ml streptavidin (dissolved in 5% BSA) for 30 min; three washes with PBS; incubation with ~0.4 nM of biotinylated Cy3-labeled DNA origami structures (dissolved in 5% BSA) for 1 h; three washes with PBS. Finally, imager strands were added in buffer C for image acquisition.

Imaging conditions. For surface-bound origami in **Supplementary Figure 9**, 12 nM Atto 655-labeled imager strands in buffer C were used. The CCD readout bandwidth was set to 5 MHz at 16 bit and 5.1 pre-amp gain with 255 EM gain was used. Imaging was performed using highly inclined (HILO) illumination³⁶ with an excitation intensity of ~23 mW using the 647 nm laser line.

Data analysis. Super-resolution images were reconstructed as described above. Here, ROI selection for qPAINT was performed in a semi-automated fashion. In brief, the co-localization between diffraction-limited and DNA-PAINT images was used to select the structures (ROIs) bound to the membrane of the cells.

Then, diffraction-limited and super-resolved images were aligned by computing the cross-correlation between them and discarding non-co-localizing molecules. After selection, qPAINT quantification was performed as described above. As before, the probe influx rate was determined by assuming that the 12 binding site origami structures carry on average 10.5 binding sites (determined by visual counting of similar structures in **Fig. 2b**). Here, a probe influx rate of 0.02163 s^{-1} was determined, resulting in an association rate of $k_{\text{on}} = 1.78 \times 10^6 \text{ M}^{-1}\text{s}^{-1}$ under these imaging conditions.

Sample preparation, acquisition, and analysis of DNA origami microinjected into fixed cells. *Sample preparation.* DNA origami structures with 44 binding sites for DNA-PAINT and fixed Cy3-labeled strands were injected into fixed HeLa cells using a Femtojet (Eppendorf, NY). Multiple injections per cell were performed into nuclear and cytoplasmic regions with the origami sample at $\sim 1 \text{ nM}$ concentration. The incorporation of the structures inside the cells was confirmed by confocal microscopy (**Supplementary Video 1**) and by deconvolution of a wide-field image stack using Huygens Professional image processing software (**Supplementary Video 2**).

Imaging conditions. For microinjected DNA origami in **Supplementary Figure 9**, 5 nM 655-labeled imager strands in buffer C were used. The CCD readout bandwidth was set to 3 MHz at 14 bit and 5.1 pre-amp gain with no EM gain was used. Imaging was performed using HILO illumination with an excitation intensity of $\sim 50 \text{ mW}$ using the 647 nm laser line.

Data analysis. Super-resolution DNA-PAINT images were reconstructed as described above. For qPAINT analysis, DNA origami structures in the cytoplasm were separated from structures in the nucleus by using the DAPI signal for segmentation (**Supplementary Fig. 9**). After structure selection, quantification was done as described above in order to determine hybridization kinetics for DNA-PAINT probes in nuclear and cytoplasmic regions. For calculating the number of binding sites, the same association rate determined in experiments on cell surfaces ($k_{\text{on}} = 1.78 \times 10^6 \text{ M}^{-1}\text{s}^{-1}$) was used, resulting in a probe influx rate of 0.0089 s^{-1} . We used the same apparent association rate, as imaging and buffer conditions are the same as in the cell surface experiments.

Sample preparation, image acquisition, and analysis of qPAINT applied to NPCs. *Sample preparation.* The nucleoporin Nup98 was labeled using a custom DNA-conjugated monoclonal antibody. In brief, first a 5'-thiolated DNA-PAINT docking strand (p1 sequence) was reduced with DTT and purified using NAP5 columns from GE Healthcare (Pittsburgh, PA). In a second step, the monoclonal antibody (#2598, Cell Signaling) was cross-linked with a 50 \times excess of a maleimide-PEG-succinimidyl ester crosslinker (746223, Sigma-Aldrich). Excess of linker that did not react with antibody was removed using Zeba columns (89883, Life Technologies). Third, the antibody-linker was reacted with the reduced 5'-thiolated DNA-PAINT docking strand at 4 $^{\circ}\text{C}$ overnight. Finally, after conjugation, the oligo-labeled antibodies were purified by using 100 kDa Amicon ultra filter (UFC510096, Emdmillipore) from unreacted DNA. The sample was then characterized by mass spectrometry, determining that on average each antibody is coupled with two docking strands.

U2OS cells were cultured in DMEM supplemented with 10% FBS. Immunostaining was performed using a standard protocol³⁷. Cells were grown overnight on 8-well Lab-Tek Chambered Coverglass. The cells were then rinsed with 2.4% PFA for 20 s in PBS and extracted with 0.4% Triton X-100 in PBS for 3 min. Next, the cells were fixed for 30 min with 2.4% PFA in PBS, quenched for 5 min with 50 mM NH₄Cl, then extensively washed with PBS (3 \times , 10 min each), and blocked with 5% BSA in PBS (blocking buffer) for 1 h. Subsequently, the cells were incubated overnight at 4 $^{\circ}\text{C}$ with the DNA-conjugated monoclonal antibody freshly diluted in the blocking buffer and then incubated with DAPI plus drift markers for 5 min. Then cells were washed once with buffer C before imaging and, finally, imager strands were added in buffer C for image acquisition.

Imaging conditions. For **Figure 3a**, 5 nM Cy3B-labeled imager strands in buffer C were used. The CCD readout bandwidth was set to 3 MHz at 14 bit and 5.1 pre-amp gain with no EM gain. Imaging was performed using HILO illumination with an excitation intensity of $\sim 8 \text{ mW}$ using the 561 nm laser line. 15,000 frames at 5 Hz frame rate were acquired.

Data analysis. Super-resolution DNA-PAINT images were reconstructed as described above. For qPAINT analysis, NPC structures in the nucleus were masked from the signal in the cytoplasm using the DAPI signal. Single Nup98 proteins or complete structures were masked using particle filter and automatic structure selection. Quantification was done as described above in order to determine hybridization kinetics for DNA-PAINT probes. The association rate was determined by using the mean value from the Gaussian fitting of the dark time distribution from the individual protein locations (see arrows in **Fig. 3a**) to $k_{\text{on}} = 1.75 \times 10^6 \text{ M}^{-1}\text{s}^{-1}$, resulting in a probe influx rate of 0.00875 s^{-1} . This value was then used to perform all qPAINT calculations.

Distances between each individual Nup98 protein in an NPC were determined by first calculating the coordinates of the center for each structure using circular Hough transform. Then we projected the histograms for the cluster of localization from the center forming a linearized intensity profile with a given number of peaks (3–7 spots, see **Supplementary Fig. 10**). Distances between spots were calculated by fitting the histograms with minimal number of Gaussians, and calculating the intervals between the peaks. This routine was implemented using custom-written MATLAB software.

Sample preparation, image acquisition, and analysis of qPAINT for quantifying Brp proteins in CAZ-units. *Sample preparation.* The Brp protein was labeled using a monoclonal antibody Brp^{Nc82} (nc82, DSHB). For DNA-PAINT, we used custom secondary anti-mouse goat-DNA-labeled antibodies. The secondary antibody was labeled using the same protocol used for the conjugation of the Nup98 antibody.

Drosophila crawling third instar larvae fillets were prepared by dissection in ice-cold HL-3.1 and fixed for 10 min using 4% paraformaldehyde in HL-3.1. The fillets were then permeabilized with 3 washes of 15 min each in PBT (PBS with 0.05% Triton X-100) followed by a 30 min block in PBT containing 1% normal goat serum and 2% BSA. Preparations were incubated with primary antibodies at 4 $^{\circ}\text{C}$ overnight. After one short and three ~ 20 min washing steps, the fillets were incubated with secondary DNA conjugated antibodies for 2 h followed by another

three washing steps. Then fillets were washed once with buffer C before imaging and, finally, imager strands were added in buffer C for image acquisition.

Imaging conditions. For **Figure 3d**, 10 nM Cy3B-labeled imager strands in buffer C were used. The CCD readout bandwidth was set to 3 MHz at 14 bit and 5.1 pre-amp gain with no EM gain. Imaging was performed using HILO illumination with an excitation intensity of ~8 mW using the 561 nm laser line. 15,000 frames at 10 Hz frame rate were acquired.

Data analysis. Super-resolution DNA-PAINT images were reconstructed as described above. For qPAINT analysis, DNA-PAINT signal from synaptic boutons on neuromuscular junctions (NMJ) were masked using anti horseradish peroxidase (HRP-A488). Single Brp molecules or complete CAZ-units were masked using particle filter and automatic structure selection. Quantification was done as described above in order to determine hybridization kinetics for DNA-PAINT probes. The association rate was determined by using the mean value from the Gaussian fitting of the dark time distribution from the individual Brp molecule locations (see **Fig. 3d** green circles) resulting in a probe influx rate of 0.0023 s^{-1} . This value was then used to perform all qPAINT calculations on individual CAZ-units. This routine was implemented using custom-written MATLAB software.

Sample preparation, acquisition, and analysis of smRNA-FISH in fixed cells.

Sample preparation. SUZ12 mRNAs molecules were tagged in fix HeLa cells using single-stranded oligonucleotides in a FISH-like hybridization scheme. mRNAs were labeled with a unique set of 64 DNA single strand oligonucleotides (**Supplementary Table 8**). Each probe consists of a unique binding sequence to the mRNA (20 nucleotides length), Cy3B coupled to the 5'-end. The 3'-end carries a single-stranded extension for DNA-PAINT (**Fig. 3f**). For coupling, the oligonucleotides were ordered with 5'-amino modifications from IDT (Coralville, IA). Cy3B was ordered as a succinimidyl ester derivative from GE Healthcare (Pittsburgh, PA). After coupling, the dye-labeled DNA strands were purified by using high pressure liquid chromatography²⁸. To perform RNA-FISH, we followed a standard protocol²⁹. Cells were fixed with pre-chilled methanol ($-20 \text{ }^{\circ}\text{C}$) for 30 min. Following fixation, cells were hybridized with the probes at 16 mM each in hybridization buffer consisting of 10% formamide, $2\times$ SSC, and 10% dextran sulfate (w/v). Samples were then hybridized overnight in a humidified chamber at $37 \text{ }^{\circ}\text{C}$. Following hybridization, samples were washed twice with wash buffer ($2\times$ SSC with 10% formamide) for 30 min at $37 \text{ }^{\circ}\text{C}$, and then incubated with DAPI plus drift markers for 5 min. Then cells were washed once with buffer C before imaging and, finally, imager strands were added in buffer C for image acquisition.

Imaging conditions. For **Figure 3f**, 5 nM Atto 655-labeled imager strands in buffer C were used. The CCD readout bandwidth was set to 3MHz at 14 bit and 5.1 pre-amp gain with no EM gain was used. Imaging was performed using HILO illumination with an excitation intensity of ~50 mW using the 647 nm laser line.

Image analysis. Super-resolution DNA-PAINT images were reconstructed as described above. Here, Bright field and DAPI images were used to identify individual cells. Diffraction-limited Cy3B and DNA-PAINT images were used to detect RNA transcripts. For image processing, a binary brightfield image was merged with a binary DAPI image. The resulting mask was used to segment the cells. Diffraction-limited spots were detected using a script that operates as follows: First, a median filter followed by a Laplacian filter was applied to each image. Then, a threshold was selected to detect individual spots. This procedure enabled us to identify the total number of diffraction-limited spots within each cell. For quantification of diffraction-limited and super-resolved images, they were aligned by computing the cross-correlation between them. After selection, qPAINT quantification was performed as described above for each individual spot in order to determine the number of probes bound to each individual mRNA. For calculating the number of binding sites, the same association rate determined previously ($k_{\text{on}} = 1.78 \times 10^6 \text{ M}^{-1}\text{s}^{-1}$) was used, resulting in a probe influx rate of 0.0089 s^{-1} . We used the same apparent association rate as imaging and buffer conditions are the same as in the experiments in **Supplementary Figure 9**.

Drift correction. *In vitro* imaging. Drift correction was performed with the custom-written MATLAB software²¹. The positions of all DNA origami structures were tracked throughout the duration of each movie and averaged for use as the drift correction trace. In the 20 nm grid super-resolution image (**Fig. 2b**), an advanced drift correction algorithm²¹ was performed to visually separate the individual grid points.

In situ imaging. For cellular imaging, 100 nm gold nanoparticles (Sigma-Aldrich; 10 nM in buffer C, added before imaging) were used as drift markers. The gold nanoparticles adsorb non-specifically to the glass bottom of the imaging chambers. Drift correction is performed in a similar fashion as for the *in vitro* imaging (see above). The apparent "movement" of all gold nanoparticles in a field of view is tracked throughout the movie. The obtained trajectories are then averaged and used for global drift correction of the final super-resolution image.

35. Hoops, S. *et al. Bioinformatics* **22**, 3067–3074 (2006).

36. Tokunaga, M., Imamoto, N. & Sakata-Sogawa, K. *Nat. Methods* **5**, 159–161 (2008).

37. Szymborska, A. *et al. Science* **341**, 655–658 (2013).